Journal of Vacuum Science and Technology A

RESEARCH ARTICLE | APRIL 01 2024

Bismuth surfactant enhancement of surface morphology and film quality of MBE-grown GaSb(100) thin films over a wide range of growth temperatures

Special Collection: Molecular Beam Epitaxy

T. Pan Menasuta ; Kevin A. Grossklaus ; John H. McElearney ; Thomas E. Vandervelde

J. Vac. Sci. Technol. A 42, 032703 (2024)
https://doi.org/10.1116/6.0003458

JVST A
Journal of Vacuum Science & Technology A

ARTICLE

pubs.aip.org/avs/jva

Bismuth surfactant enhancement of surface morphology and film quality of MBE-grown GaSb (100) thin films over a wide range of growth temperatures

Cite as: J. Vac. Sci. Technol. A **42**, 032703 (2024); doi: 10.1116/6.0003458
Submitted: 15 January 2024 · Accepted: 8 March 2024 ·
Published Online: 1 April 2024

T. Pan Menasuta,[a] Kevin A. Grossklaus,[b] John H. McElearney,[c] and Thomas E. Vandervelde[d]

AFFILIATIONS

Renewable Energy and Applied Photonics Labs, Department of Electrical and Computer Engineering, Tufts University, 61 College Ave, Medford, Massachusetts 02155

Note: This paper is a part of the Special Topic Collection on Molecular Beam Epitaxy.
[a]**Author to whom correspondence should be addressed:** thachachanok.menasuta@tufts.edu
[b]**Electronic mail:** kevin.grossklaus@tufts.edu
[c]**Electronic mail:** john.mcelearney@tufts.edu
[d]**Electronic mail:** tvanderv@ece.tufts.edu

ABSTRACT

We investigate the surface morphologies of two series of homoepitaxial GaSb(100) thin films grown on GaSb(100) substrates by molecular beam epitaxy in a Veeco GENxplor system. The first series was grown at temperatures ranging from 290 to 490°C and serves as a control. The second series was grown using the same growth parameters with bismuth used as a surfactant during growth. We compared the two series to examine the impacts of bismuth over the range of growth temperatures on the GaSb surface morphologies using atomic force microscopy and the film properties using Raman spectroscopy and scanning electron microscopy. High-resolution x-ray diffraction was performed to confirm that bismuth was not incorporated into the films. We found that the morphological evolution of the GaSb series grown without bismuth is consistent with the standard surface nucleation theory and identified the 2D-3D transition temperature as close to 290° C. In contrast, the presence of a Bi surfactant during growth was found to significantly alter the surface morphology and prevent undesired 3D islands at low temperatures. We also observed a preference for hillocks over step morphology at high growth temperatures, antistep bunching effects at intermediate temperatures, and the evolution from step-meandering to mound morphologies at low temperatures. This morphological divergence from the first series indicates that bismuth significantly increases in the 2D Erlich–Schwöebel potential barrier of the atomic terraces, inducing an uphill adatom flux that can smoothen the surface. Our findings demonstrate that bismuth surfactant can improve the surface morphology and film structure of low-temperature grown GaSb. Bismuth surfactant may also improve other homoepitaxial III-V systems grown in nonideal conditions.

I. INTRODUCTION

Epitaxial growth of GaSb is critical for emerging mid-infrared optoelectronic technology, including thermal imaging, optical communications, light-emitting diodes (LEDs), and thermophotovoltaic (TPV) cells.[1–5] While GaSb films are typically grown around 450°C, lower growth temperatures can be favorable for several reasons, ranging from compatibility with other layers that can require low temperature growth to lower bulk mobility to prevent defects.[51] The surface of GaSb degrades with lower growth temperatures, which can lead to surface defects and degradation of device performance. As the growth temperature decreases, the growth transitions from layer-by-layer to Stranski–Krastanov (SK) and eventually to the rough 3D islanding regime.[6,7,51] Furthermore, systematic characterization of homoepitaxial GaSb surfaces has not

been carried out at temperatures beyond the range of 350–450°C, not to mention in the presence of a surfactant.[8,51]

The use of surfactants in thin-film epitaxial growth to suppress 3D islanding is well known and has been cataloged for dozens of semiconductor film, substrate, and surfactant combinations.[9,51] In particular, bismuth has been used as a surfactant to enhance the surface morphology during the growth process of several III-V materials.[10,51] The surface desorption rate of bismuth is low due to its low vapor pressure. As a result of its large size, the incorporation of bismuth into the film is not favorable in terms of energy and strain.[11] Thus, the bismuth atoms segregate on the growth surface and remain there long enough to act as a surfactant, modifying the surface morphology. Various works on bismuth-containing alloys have also reported the benefits of the bismuth surfactant.[11–20] However, there are no studies on the use of Bi surfactant in homoepitaxial GaSb thin films.[21,22,51]

There are currently two major theories on the microscopic mechanism of this surfactant's suppression 3D-islanding effect. The traditional approach is to explain the effects in terms of the adatom diffusion and attachment processes whose treatments are mostly isotropic and independent of the nanostructure.[23–26,51] However, this approach loses validity in highly anisotropic systems and/or in the presence of significant step-edge and step-corner Ehrlich–Schwöebel (hereby ES) barriers.[23,27] The kinetics quickly becomes highly complex, as adatoms experience different types and amounts of potential, depending on both the vicinal structures and the locations of the adatoms.[28] A more appropriate approach to characterizing the surface morphologies over a wide range of growth conditions is to expand beyond the "transient" regions, which can be described by the step-flow or the sticking pictures. In their comprehensive work, Villain proposes that in many scenarios, adatom diffusion is governed by asymmetric potential barriers at the microscopic level step edges.[29]

Bales and Zangwill validated the importance of the asymmetry of the step edges that led to the discovery of the Bales–Zangwill instability.[30] Thus, nonequilibrium growths, which are present in our study, are better explained from the perspective of potential barriers.[23] This thin-film growth picture has also been called the modified terrace step kink model (modified TSK) and the Wolf–Villain Erlich–Schwöebel (WV-ES) model.[24,31] To avoid confusion, we will refer to this particular framework as the Erlich–Schwöebel picture. Although the model has been introduced and justified for a few decades, it has recently gained more acceptance with the availability of atomic-level observation, such as STM, and advances in complex growth simulation, such as kinetic Monte Carlo (kMC).[24,32] A number of simulation works demonstrate that a significantly high 2D (ES) barrier is required for the nonequilibrium growth morphologies—e.g., step-meandering, mounding, and other 3D nanostructures—to occur.[32–36] While there have been other proposed mechanisms of these morphologies, the ES picture is the most consistent with observations in many relevant systems.[6,23,37–39,51]

This work examines the effects of the bismuth surfactant on different types of ES potential barriers and its impacts on the surface morphology of homoepitaxial GaSb by comparing the surfactant-mediated surfaces with the control series grown without bismuth over a wide range of growth temperatures. Specifically, the focus will be on the two-dimensional Erlich–Schwöebel (2D ES) barrier or the step Erlich–Schwöebel effects (SESEs). This potential decreases the probability of adatoms diffusion down a step. The 2D ES barrier, when combined with the classical potential between steps, results in asymmetric potential barriers and subsequent tunneling or diffusion bias.[27] In other words, the potential asymmetry effectively creates an uphill diffusion bias, increasing the likelihood of nonequilibrium morphologies and nanostructure formation.[37,38] This is the most common ES barrier and is often without specifying the dimensionality. The one-dimensional Erlich–Schwöebel (1D ES) will also be touched upon. This type of ES barrier is also known as the kink Erlich–Schwöebel effect (KESE) or the cornering barrier.[40,41] As the name suggests, adatoms can be prevented from cornering between adjacent step edges in the presence of the 1D ES barrier. This type of ES barrier can affect the straightness of the step edge and the formation of kinks.[29,40] Finally, the three-dimensional Erlich–Schwöebel (3D ES) which prevents adatoms motion between facets, e.g., 111–100, is not observed and is beyond the scope of this study.[42]

In this study of GaSb, surfaces with a high complexity of features and nanostructures are seen that lie between 2D and 3D. This mesoscopic-scale analysis treats some processes (such as step flow) as a continuum, while treating others (such as nanostructures) as individuals.[38] As will be discussed in Sec. III B, the Erlich–Schwöebel picture allows us to distinguish and characterize the impacts of bismuth surfactants on different aspects of structures and avoid excessive macroscopic simplification. Therefore, we will not attempt to conclude the impacts of surfactants on the kinetic parameters typically associated with classical models, such as diffusion lengths.

II. EXPERIMENTAL PROCEDURES

GaSb samples were grown in a Veeco GENXplor MBE system on quarter pieces of 2-in., p-doped (100) oriented GaSb substrates. Each sample was heated for oxide removal at 560°C under Sb overpressure. The initial appearance of spots and then a brightening in the reflection high-energy electron diffraction (RHEED) pattern indicate full oxide desorption. The beam equivalent pressures (BEPs) were determined prior to growth using a beam flux monitor (BFM). The Ga flux was chosen to achieve a growth rate (GR) of 0.4 ML/s as measured by RHEED intensity oscillations (RIOs). The Sb flux was then set 20% above the stoichiometric point, determined by watching for a change in the shape of the GaSb RIO while decreasing the Sb flux. On our system, that point is at a measured Sb:Ga BEP ratio of ∼0.7. A 100 nm of GaSb buffer layer was then deposited at 490°C at the growth rate of ∼0.4 monolayers per second (ML/s) to smoothen the surface. The 200-nm GaSb layer of interest is then grown on the buffer layer at varying growth temperatures. Front-side temperatures above ∼400 °C were measured by blackbody spectroscopy using a k-Space Associates BandiT system. For temperatures below that, a trend relating substrate heater set-point and measured blackbody temperature was determined and extrapolated. This was done by lowering the heater set-point in 10°C steps until the BandiT was unable to accurately read the growth surface temperature. To help push that minimum to lower temperatures, background spectra

were taken for each sample, with the sample cold (< 200°C) and the Sb shutter open (typically the hottest source with its 900°C cracker). The samples were rotated at 20 rotations per minute (RPM) during growth to improve the uniformity of the film across the substrate. Series A was grown without Bi and Series B with Bi as a surfactant using an Sb:Bi BEP ratio of 10. The growth temperature for each series varied from 290 to 490°C in 40°C steps, resulting in six samples for each of the two series.

In this study, we focus on the effect of Bi surfactant on the surface morphologies at different growth temperature points to examine the effects of the surfactant on the ES barriers. Atomic force microscopy (AFM) was performed in a tapping mode to characterize the surface morphologies using an Asylum Research Cypher S microscope. As In-free mounting can lead to temperature gradients across the sample surface during growth, AFM images were taken at two distinct locations across the wafer for each temperature for comparison. All AFM data analysis and plotting were performed in the Gwyddion software. Minimal 2D Fourier noise filtering, scar removal, and polynomial background removal were performed to process the AFM data. The samples will be referenced by growth temperature, followed by series, e.g., 490A for the sample grown at 490°C from series A.

Since bismuth incorporation increases at lower temperatures, high-resolution x-ray diffraction (HRXRD) (004) $2\theta\ \Omega$ line scans and rocking curves were performed using a Bruker D8 x-ray diffractometer to confirm that incorporation is negligible, that is, less than 1% of group V sites. The simulations were performed using the Bruker Leptos software package.

To infer the crystalline quality of all of the samples, Raman spectroscopy was performed using a Horiba Multiline Raman Spectrometer with a 532 nm laser. LabSpec software suite was used to analyze the shifted spectra. Additionally, samples are characterized by variable-angle spectroscopic ellipsometry (VASE) using a J.A. Woollam VASE UV-NIR Spectroscopic Ellipsometer. Full-spectral (200–2500 nm at 5 nm steps) scans for changes in the refractive index and fine scans (1600–1900 nm at 2 nm steps) covering the bandgaps were performed.

Finally, to confirm the 3D islanding transition of the sample grown at 290°C without bismuth surfactant, scanning electron microscopy (SEM) and energy-dispersive x-ray spectroscopy (EDS) were performed using a Zeiss GeminiSEM 360 instrument.

III. RESULTS AND DISCUSSION

A. Series A (no Bi) morphology

The left columns of Figs. 1 and 2 show the surface topology of GaSb films grown without Bi surfactant over a wide range of decreasing growth temperatures. This control series follows the standard surface nucleation theory quite well. As depicted in Fig. 1(c), the surface of sample 450A exhibits the 2D layer-by-layer growth (Frank–van der Merwe) at the high growth temperature. On the contrary, Fig. 2(e) shows the rough 3D island growth (Volmer–Weber) of sample 290A grown at the low growth temperature. The rest of the samples in Series A exhibit intermediate Stranski–Krastanov (SK) growths, which are layer-by-layer growths with some very flat 3D structures, the so-called 2.5D growth regime.[25] This subsection will discuss the surface morphologies

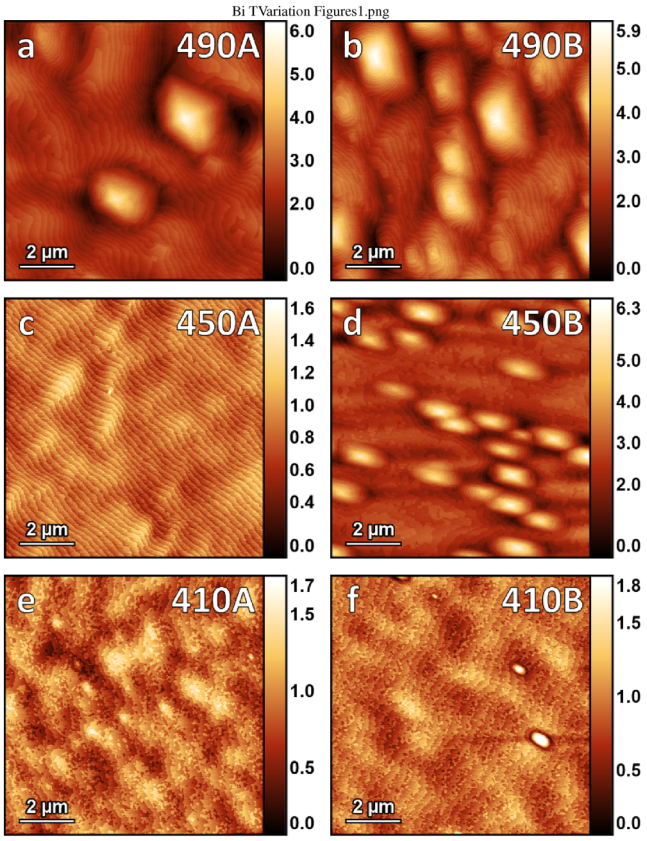

FIG. 1. AFM topographs of GaSb films of samples (a) 490A, (b) 490B, (c) 450A, (d) 450B, (e) 410A, and (f) 410B with a field of view of 1 μm and height bars in nm.

from growth temperatures of 490–290°C and show that their morphological evolution follows the standard equilibrium growth theory.

The surface morphology of sample 490A [Fig. 1(a)] is indicative of diffusive step flow, with a terrace width of approximately 200 nm. At high temperatures, the energetic adatoms have high mobility, such that they can migrate across the surface and reach steps for attachment and step formation.[25] As can be seen in Fig. 1(a), the step edges are not straight and contain kinks. The presence of kinks suggests that the adatoms have excess energy. In particular, the growth temperature is higher than the critical temperature and the probability of kink formation is high.[25] At sufficiently high density of positive (forward) kinks, the adatoms settle further away from the step edges to maximize the number of near neighbors.[25] By chance, this leads to the formation of 2D islands. In the presence of 2D ES barriers and large islands, adatoms form "hillocks" structures; see an example in Fig. 3.[8] After a certain number of concentric monolayers, the hillocks become self-stabilized and self-similar, possessing a regular step width and maximum vertical and lateral heights indicative of equilibrium structures.[8,37,43,44] Larger FOV images show that the surface of

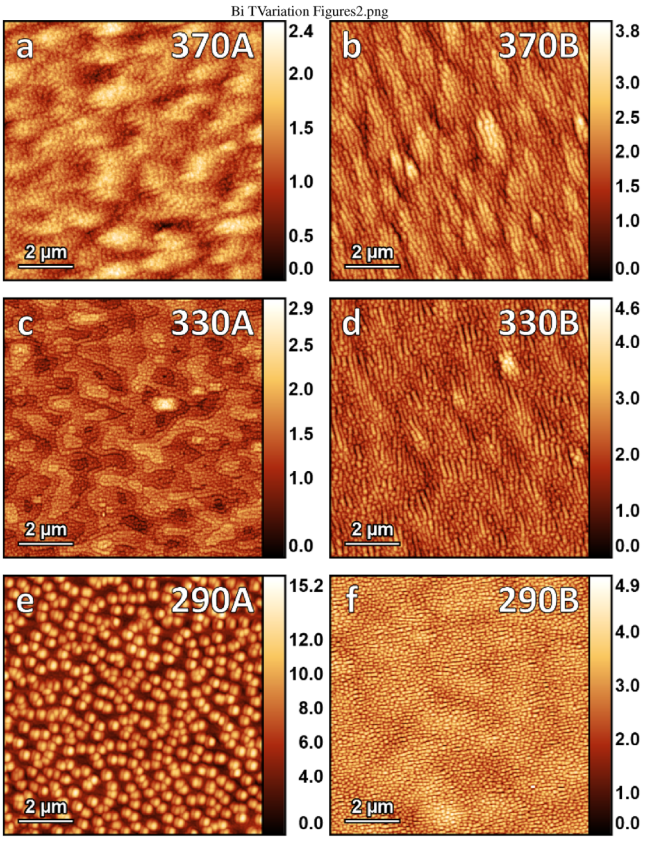

FIG. 2. AFM topographs of GaSb films of samples (a) 370A, (b) 370B, (c) 330A, (d) 330B, (e) 290A, and (f) 290B with a field of view of 1 μm and height bars in nm.

490A contains approximately 30 hillocks, ~ 8–10 of which are mature, with a scan size of $20 \times 20\,\mu m^2$. This corresponds to a surface density of approximately $7.5 \times 10^6\,cm^{-2}$.

Sample 450A, shown in Fig. 1(c), also shows the diffusive step flow morphology grown at 450°C with straight edges of width ~ 200 nm and mostly free of kinks. This agrees well with Okumura *et al.* who use 440°C growth temperature, GR = 0.33 μm/h, Sb:Ga BEP ratio = 10:1, and GaSb 0.35° off (100) substrates; and Nosho *et al.* who use 450°C growth temperature, GR = 0.5 ML/s, Sb:Ga BEP ratio = 2:1.[8,45] Again, the coverage of the adatoms is high and facilitates the flow process. This is the preferred surface morphology for high thin film quality.[25,51]

The morphology of the surface sample 410A, depicted in Fig. 1(e), is the convective step flow. With a relatively colder growth temperature of 410°C, adatoms are slow and their diffusion is on the order of step flow velocity.[25] Note that the step velocity and width oscillate along the step flow direction, generating a pattern unique to this morphology. The acceleration is the result of the step consuming the adatoms that build up in clusters on large terraces. Then the step slows down and repeats. There are two types of bunching, convex and concave, corresponding to the relative

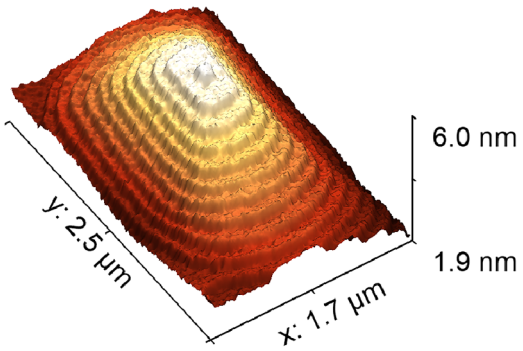

FIG. 3. 3D topography of a hillock structure from sample 490B.

velocity between the slow step and diffusion.[38] Whether the bunching is convex or concave is unclear from our AFM data. For this sample, the average terrace width is about 300 nm and the bunching oscillates with a period of 2–3 μm.

Figure 2(a) shows the morphology at a lower growth temperature of 370°C, the adatoms have even less energy. The adatom diffusion of sample 370A is much slower than the step flow and the adatom arrival rate. Slow adatoms have little mobility and prefer to settle in clusters near their landing zones. The layers are formed by 2D islands (~ 100 nm) merging in the process known as coalescence.[25] This morphology is known as the 2D island morphology.[25]

The unusual surface morphology of sample 330A grown at 330 °C shown in Fig. 2(c) exhibits 2D islandlike nucleation sites that coalesce into larger irregular steplike terraces with round edges. Note that this morphology manifests well below both step-flow and 2D-island temperatures, implying that this is a completely different morphology. The low growth temperature, combined with the high-density nucleation islands and the irregular roundness of the terraces somewhat resemble the rarely observed "loch-keime" morphology of the island type.[26] Although the physics of this morphology is not well understood, it has been thought to be caused by supersaturation at very low growth temperatures, which is also the growth condition of this sample.[26] The morphology simulates layer growth through periodically symmetric islands coalescing into pseudo-steps of corallike shape.

Finally, Fig. 2(e) clearly shows the abrupt transition to the rough 3D growth regime near 290°C.[7] We observe that the 3D islands are twin cornlike 3D structures. SEM and EDS data do not show significant differences in elemental composition. The observed droplets do not differ compositionally from the rest of the surface. The presence of 3D islands indicates that the film was grown below the critical temperature, and the surface breaks up into large 3D regions. Each droplet is ~ 0.4 μm in diameter and ~ 10 nm in height. The density of 3D structures is estimated to be ~ 400–500 at a scan size of $10\,\mu m \times 10\,\mu m$, corresponding to a surface density of approximately $4 - 5 \times 10^8\,cm^{-2}$.

Therefore, we have a complete picture of the morphological evolution of GaSb over a wide range of growth temperatures of 490–290°C. We also demonstrate the agreement between our control series and the standard equilibrium nucleation theory. The

morphology evolves from step-flow to 2D islanding to 3D islanding as growth temperatures are decreased. The 2D-3D transition point is identified as near 290 °C. The presence of hillocks on 490A has also been observed by Murray *et al.* and is an indicator that GaSb has a positive, albeit small, 2D ES barrier.[43] However, for growth temperatures of 290–410 °C, the barrier's effects are observed to have become negligible or dominated by other processes.

B. Series B (with Bi) morphology and comparison to series A

Samples in Series B are grown under the same growth parameters, e.g., substrates, fluxes, growth temperatures, with the addition of a very low Bi flux (Sb:Bi BEP ratio of 10). The large bismuth atoms, which normally are challenging to incorporate into the GaSb lattice, modify the surface morphology during growth. The right column of Figs. 1 and 2 show samples from series B. Compared to series A, the Bi surfactant clearly alters the surface morphologies of GaSb thin films for all growth temperatures depicted. An immediately observable result is the suppression of 3D island formation at a growth temperature of 290 °C [Fig. 2(f)]. This subsection will discuss the surface morphologies from the samples of series B, again in the order of descending growth temperatures, to compare the surface morphologies with those of series A and discuss the increase in ES barriers by Bi surfactant seen across different growth temperatures (Fig. 4).

The surface morphology of 490B, as depicted in Fig. 1(b), bears some similarities to that of 490A except for the significant increase in hillock formation of density ∼ 60 hillocks at the 20 μm area scale, vs ∼ 30 of 490A). This is expected because the adatoms are highly energetic at this growth temperature. However, instead of being available to facilitate step-flow growth, it can be observed

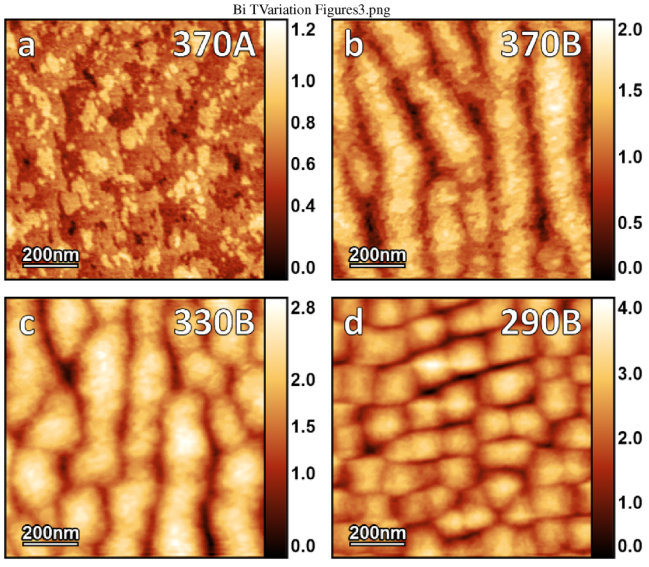

FIG. 4. AFM topographs of GaSb films of samples (a) 370A, (b) 370B, (c) 330B, and (d) 290B with a field of view of 1 μm and height bars in nm.

that hillock growth is the preferred morphology, instead of step-flow, in the presence of bismuth. We attribute this preference to the increase in the 2D ES barrier. With an increase in the energy barrier, adatoms have a lower and unequal probability of going to lower steps. This result is consistent with Johnson *et al.*'s simulation epitaxial GaAs with high 2D ES barriers.[23] Again, the distinct appearances of the matured hillocks—e.g., self-similarity, regular-width steps, and maximum lateral and vertical sizes—are observed, consistent with the self-stabilization effects seen by Murray *et al.*[43]

Sample 450B, shown in Fig. 1(d), exhibits unusually wide terraces, ∼ 300–1000 nm, uniformly scattered with hillocks, ∼ 80 hillocks at 20 μm area scale. As is evident from the straight diffusive step flow morphology of sample 450A, the adatoms are very energetic at this temperature, and their ability to migrate and move large distances across the growth surface is high. Wide terrace widths of 300 nm to 1 μm, compared to 200 nm of 450A, also support this conclusion. Similarly to sample 490A, hillocks are the preferred morphology in the presence of bismuth, which we ascribe to the increased 2D ES barrier. Once adatoms diffuse up the hillocks, they have a lower probability of going down. Thus, the adatoms feed into hillocks constructed of a relatively large quantity of atoms rather than steps. It is possible that the difference in the width of the atomic terrace may be a result of differences in the effective off-cut angles of the samples. Specifically, a 200-nm terrace suggests an off-cut of roughly 0.1°, while a 1000 nm terrace implies an off-cut of around 0.02°. Both values fall within the accepted ranges for both wafer cutting and postpolishing surface flatness.

Figure 1(f) shows sample 410B. Both 410A and 410B exhibit a convective step flow morphology. In particular, the step widths of 410B are much more equal with ∼ 300 nm width. This "antistep bunching" or "step-equalization" effect is also observed when bismuth is used as a surfactant during the GaAs epitaxy by Hassanen *et al.*[10] The authors cite this as the surfactant promoting uphill attachment. The favored uphill attachment causes larger terraces to shrink faster than smaller ones.[10] Furthermore, the gaps around the hillocks confirm the self-stabilizing nature of the hillocks, similar to what is observed in 450B.

At the lowered growth temperatures of 370 and 330 °C, we observed a significant divergence in morphology from series A. Specifically, samples 370B [Fig. 2(b)], 330B [Fig. 2(d)], and 290B [Fig. 2(f)] follow the nonequilibrium morphological evolution from "step-meandering" to "mound" structures. This morphological evolution is well known in epitaxy simulation as a result of significant ES barriers.[40] Note that the morphological instability does not imply the thermodynamic instability; the lattice is still homogeneous and growth remains in the mesoscopic 2.5D/SK regime.[23,40]

Both samples 370B [Fig. 2(b)] and 330B [Fig. 2(d)] exhibit a step-meandering morphology (see Fig. 5). In the absence of the 2D ES barrier, the adatoms prefer to attach to the edges of the terraces. The diffusion bias from the high 2D ES barrier induces an effective "uphill" current, which causes the advanced terraces to accelerate.[36,38] This phenomenon is also known as the Bale–Zangwill (BZ) instability. This fluctuation results in the observed rippling "fjord" structures, which is a nonequilibrium 2.5D/SK growth. The steps of both samples meander at a period of approximately 200 nm. The shorter lengths of the fjords seen at 330 °C than at 370 °C indicate

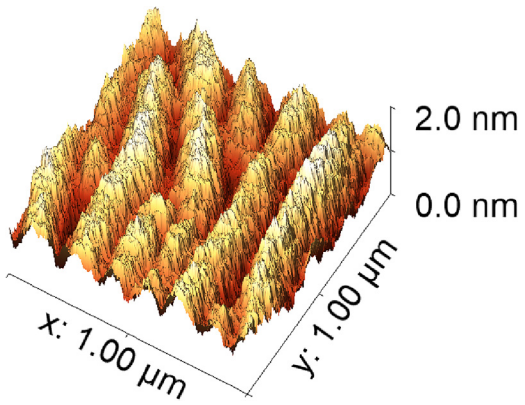

FIG. 5. 3D topography of the step-meandering structures from sample 370B.

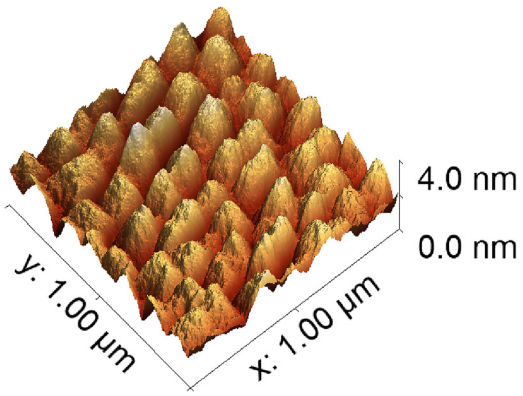

FIG. 6. 3D topography of the mound structures from sample 290B.

more meandering effects, since adatoms have lower energy at 330 °C. Furthermore, the fjords of sample 370B are taller. We also observed the pinching of the fjords into very short ones in 330B. This effect is a result of the secondary instability, which becomes dominant at 290 °C.

Instead of exhibiting 3D islanding like 290A, sample 290B exhibits the mound morphology, another 2.5D nonequilibrium regime that evolves from the step-meandering.[36] A second instability resulting from the 1D ES barrier dominates at the lower temperature.[40] Adatoms attach to the step, do not corner, then preferentially flow uphill and form mound structures. Unlike hillocks, the mounds' morphology lacks regularly spaced terraces indicative of equilibrium or stable growths. The fine mound structures also have a square geometry and two-dimensional periodicity, which are observed in this sample.[33,40] The mound density is estimated to be ∼ 50 on an area scale of 1 μm. Each mound is ∼ 3 nm high and ∼ 200 nm wide. It has been theoretically suggested that mounds can smooth the surface due to the small sizes of the structures.[24,40] Our results show that the Bi surfactant improves the smoothness of 290B compared to the sample 290A which contains tall fully formed 3D structures. Furthermore, the mound structures of 290B are observed to be "cuspy" – e.g., curves merging in points; see Fig. 6 – suggesting a relatively weak 1D ES barrier.[40]

C. Results from VASE, Raman spectroscopy, SEM, EDS, and HRXRD

Figures 7(b)–7(d) show the result of Raman spectroscopy. As shown in Figs. 7(b) and 7(c), there is no observable trend in the amplitude of the peak count and the Raman wavelength shift is not statistically significant. This implies that there is no significant compositional variation between series A and B. The full-width at half-maximum (FWHM) shown in Fig. 7(d) exhibits a divergence near the growth temperature of 370 °C. SEM and EDS performed on sample 290A suggest that there is no compositional variance on the surface. The ellipsometric data from series A and B show no observable differences in the optical responses. HRXRD was performed on sample 290B, which is grown at the coldest temperature and is most susceptible to alloying. The result shows a Bi fraction of 0.45% stoichiometric composition or 0.225% atomic percentage, which is well below our threshold for alloying as opposed to surfactancy. This corresponds to incorporation of at least an order of magnitude lower than the Sb:Bi BEP ratio would imply, suggesting that the rest of the Bi atoms stay on the surface, modify the surface morphology, and eventually desorb. Although we acknowledge the potential classification of some colder-grown samples as very dilute GaSbBi alloys, we maintain that the observed effects primarily stem from Bi's surfactancy behavior.

D. Roles of bismuth surfactant

As discussed in Sec. III B, the increase in the 2D ES barriers by bismuth surfactant is consistently observed over a wide range of

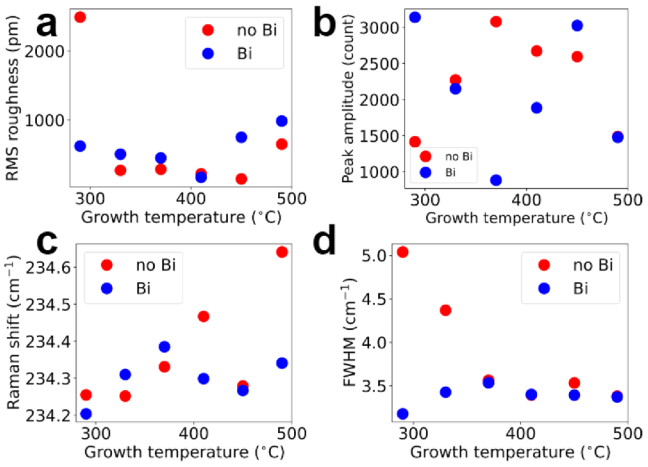

FIG. 7. Plots of (a) root-mean-square (RMS) roughness (pm) vs growth temperature (°C), (b) Raman peak amplitude (count) vs growth temperature (°C), (c) Raman peak wavenumber (cm^{-1}) vs growth temperature (°C), and (d) Raman peak full-widths at half-maximum (cm^{-1}) vs growth temperature (°C).

temperatures. The evolution from step-meandering to mounds has been well studied by simulation and experimental works to require a significant 2D ES barrier.[46,47] Although hillocks, antistep bunching, step-meandering, and geometric mounds could potentially arise from other mechanisms, their occurrence in the presence of bismuth surfactant indicates that the 2D ES potential barrier is markedly elevated by the presence of bismuth.

The root-mean-square (RMS) roughness obtained from AFM data analysis is shown in Fig. 7(a). Quantitatively, the samples in series B are slightly rougher at higher growth temperatures. A significant improvement is observed at 290°C due to suppression of 3D islanding. Figure 8 shows the normalized height distributions for the two series. Qualitatively, the trends in RMS roughness and the shapes of the height histograms are consistent with the data from Raman FWHM and the discussion of surface morphology.

It is unclear from the AFM images of samples 450A and 450B whether the 1D (cornering) ES barrier is affected. If bismuth anisotropically increased the 1D barrier, we should expect the hillock to also become more asymmetric and more rounded on two opposite sides, since the adatoms would prefer to go over the corners. Additionally, 2D islands should become compact with a low 1D ES barrier, as adatoms can corner effectively.[48] However, this morphology is not observed in the presence of Bi, thus we cannot comment on the effects of bismuth on it. Furthermore, we did not observe any clear evidence, such as facet formation, of bismuth surfactant that affects the 3D ES barrier.

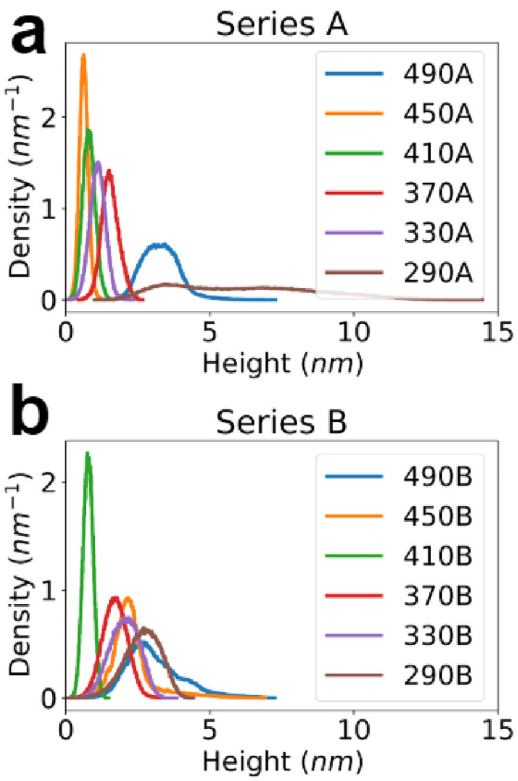

FIG. 8. Normalized height distributions: (a) series A and (b) series B.

Lui *et al.* recently observed using STM that bismuth atoms[49] agglomerate at the edge of the steps of GaAs. According to the standard strain theory, the favorable energy state for bismuth atoms is at the edge of steps, because of their larger size. We postulate that this mechanism is the physical cause of the increase in the 2D ES barrier which, by definition, is the effective barrier seen by the adatoms diffusing from an upper to a lower step.

Another recent study on Bi surfactant on MBE-grown GaAs films also emphasizes its effects on ES barriers. While the 2D ES barrier of GaAs(100) is reported to be small and negative,[50] GaAs (111) suffers from large 2D ES barriers. Hassanen *et al.* observe that bismuth surfactant increases attachment uphill while improving diffusion downhill, leading to the conclusion that Bi surfactant decreases the 2D ES barrier for GaAs(111).[10] This diverges from the conventional effects of the 2D ES barrier, where its increase would drive both the adatom fluxes uphill and the attachment to increase. This further highlights the need for systematic studies of Bi surfactants on the 2D ES barrier of other III-V semiconductors.

IV. CONCLUSION AND FUTURE WORK

We have shown and compared the morphological evolution of the GaSb series grown with and without surfactants. We also demonstrate that the control series is consistent with the standard surface nucleation theory. Bismuth surfactant was found to suppress 3D island formation at 290 °C and cause significant changes in surface morphology under other growth conditions. We discuss various morphological regimes and features that led us to conclude that bismuth increases the 2D ES potential barrier. Thus, this work serves to confirm that bismuth surfactant can be used to enhance III-V epitaxial growths under nonideal conditions.

In a recent cellular automata simulation work, the 2D ES barriers are modeled into two parts.[27] Załuska-Kotur *et al.* found that the nonequilibrium morphologies ranging from step-meandering to tall nanopillars can be controlled with the two potentials.[27] A study that uses Bi surfactant with varying fluxes to trigger these unique morphologies could be valuable for nanostructure growth.

As we observed, the greatest improvement and morphological change at 290 °C, a future study where the bismuth flux is varied at this temperature will be essential to understand how ES barriers are affected by different amounts of bismuth surfactant. For example, mound structures can become cuspier with a lowered 1D ES barrier, change patterns, or even change entirely into other morphologies.

ACKNOWLEDGMENTS

This work was supported by the Office of Naval Research (Nos. N00014-15-1-2946 and N00014-17-1-2591) and the National Science Foundation (Nos. ECCS 1930942, EECS 1806311, and ECCS 2120568). The samples were grown in the Tufts Epitaxial Core Facility (TECF) on equipment supported by NSF (No. EECS 1337783). Characterization was performed in part at Harvard University's the Center for Nanoscale Systems (CNS); a member of the National Nanotechnology Coordinated Infrastructure Network (NNCI), which is supported by the National Science Foundation

under NSF Award No. ECCS-2025158. Furthermore, this work used MRSEC Shared Experimental Facilities at MIT, supported by the National Science Foundation under Award No. DMR-1419807. We gratefully thank Chanita Tubthong for reading the manuscript and for LaTeX formatting assistance.

AUTHOR DECLARATIONS

Conflict of Interest

The authors have no conflicts to disclose.

Author Contributions

T. Pan Menasuta: Conceptualization (equal); Data curation (equal); Formal analysis (equal); Investigation (equal); Methodology (equal); Visualization (equal); Writing – original draft (equal); Writing – review & editing (equal). **Kevin A. Grossklaus:** Conceptualization (supporting); Formal analysis (supporting); Investigation (supporting); Project administration (equal); Supervision (supporting); Writing – review & editing (supporting). **John H. McElearney:** Data curation (supporting); Formal analysis (supporting); Investigation (supporting); Writing – review & editing (equal). **Thomas E. Vandervelde:** Conceptualization (equal); Funding acquisition (lead); Project administration (equal); Resources (equal); Supervision (equal); Validation (equal); Writing – review & editing (equal).

DATA AVAILABILITY

The data that support the findings of this study are available from the corresponding author upon reasonable request.

REFERENCES

[1]C. Downs and T. E. Vandervelde, Sensors **13**, 5054 (2013).
[2]A. Zayan, M. Stevens, and T. E. Vandervelde, "GaAsBi alloys for photovoltaic and thermophotovoltaic applications," in *2016 IEEE 43rd Photovoltaic Specialists Conference (PVSC)* (IEEE, Portland, OR 2016), pp. 2839–2843.
[3]D. F. DeMeo and T. E. Vandervelde, MRS Proc. **1329**, mrss11-1329-i11-10 (2011).
[4]T. N. Danilova, B. E. Zhurtanov, A. N. Imenkov, and Y. P. Yakovlev, Semiconductors **39**, 1235 (2005).
[5]A. W. Bett and O. V. Sulima, Semicond. Sci. Technol. **18**, S184 (2003).
[6]J. Krug, "Introduction to step dynamics and step instabilities," in *Multiscale Modeling in Epitaxial Growth, ISNM International Series of Numerical Mathematics*, edited by A. Voigt (Birkhäuser, Basel, 2005), pp. 69–95.
[7]M. Ohring, "Substrate surfaces and thin-film nucleation," in *Materials Science of Thin Films (2nd ed.)*, edited by M. Ohring (Academic Press, San Diego, 2002), Chap. 7. pp. 357–415.
[8]B. Z. Nosho, B. R. Bennett, E. H. Aifer, and M. Goldenberg, J. Cryst. Growth **236**, 155 (2002).
[9]D. F. Storm, M. D. Lange, and T. L. Cole, J. Appl. Phys. **85**, 6838 (1999).
[10]A. M. Hassanen, J. Herranz, L. Geelhaar, and R. B. Lewis, Semicond. Sci. Technol. **38**, 095009 (2023).
[11]T. Hepp, L. Nattermann, and K. Volz, "MOVPE growth and device applications of ternary and quaternary dilute bismide alloys on GaAs substrates," in *Bismuth-Containing Alloys and Nanostructures, Springer Series in Materials Science*, edited by S. Wang and P. Lu (Springer, Singapore, 2019), pp. 37–58.
[12]C. M. Krammel, P. M. Koenraad, M. Roy, P. A. Maksym, and S. Wang, "Structural properties of Bi containing InP films explored by cross-sectional scanning," in *Bismuth-Containing Alloys and Nanostructures, Springer Series in Materials Science*, edited by S. Wang and P. Lu (Springer, Singapore, 2019), pp. 215–229.
[13]J. M. Millunchick and C. R. Tait, "Surface mediated growth of dilute bismides," in *Bismuth-Containing Alloys and Nanostructures, Springer Series in Materials Science*, edited by S. Wang and P. Lu (Springer, Singapore, 2019), pp. 201–214.
[14]L. Wang, H. Liang, Z. Shen, and S. Wang, "Bismuth-related nanostructures," in *Bismuth-Containing Alloys and Nanostructures, Springer Series in Materials Science*, edited by S. Wang and P. Lu (Springer, Singapore, 2019), pp. 181–199.
[15]J. Zhang, Y. Wang, and J. M. O. Zide, "Dilute bismuthides on InP substrates: From materials to devices," in *Bismuth-Containing Alloys and Nanostructures, Springer Series in Materials Science*, edited by S. Wang and P. Lu (Springer, Singapore, 2019), pp. 163–179.
[16]O. Delorme, L. Cerutti, R. Kudrawiec, E. Luna, J. Kopaczek, M. Gladysiewicz, A. Trampert, E. Tournié, and J.-B. Rodriguez, "GaSbBi alloys and heterostructures: Fabrication and properties," in *Bismuth-Containing Alloys and Nanostructures, Springer Series in Materials Science*, edited by S. Wang and P. Lu (Springer, Singapore, 2019), pp. 125–161.
[17]S. Wang, T. Jin, S. Zhao, D. Liang, and P. Lu, "Phosphorus and nitrogen containing dilute bismides," in *Bismuth-Containing Alloys and Nanostructures, Springer Series in Materials Science*, edited by S. Wang and P. Lu (Springer, Singapore, 2019), pp. 97–123.
[18]P. K. Patil, S. Shimomura, F. Ishikawa, E. Luna, and M. Yoshimoto, "Strategic molecular beam epitaxial growth of GaAs/GaAsBi heterostructures and nanostructures," in *Bismuth-Containing Alloys and Nanostructures, Springer Series in Materials Science*, edited by S. Wang and P. Lu (Springer, Singapore, 2019), pp. 59–96.
[19]L. Yue, X. Zhang, W. Ou, Z. Shen, and S. Wang, "Molecular beam epitaxy growth and properties of GaAsBi and AlAsBi," in *Bismuth-Containing Alloys and Nanostructures, Springer Series in Materials Science*, edited by S. Wang and P. Lu (Springer, Singapore, 2019), pp. 11–36.
[20]P. Lu, D. Liang, X. Guan, Q. Wang, H. Zhao, and L. Wu, "Electronic properties of dilute bismides," in *Bismuth-Containing Alloys and Nanostructures, Springer Series in Materials Science*, edited by S. Wang and P. Lu (Springer, Singapore, 2019), pp. 1–9.
[21]"Bismuth-containing alloys and nanostructures," in *Springer Series in Materials Science*, edited by S. Wang and P. Lu (Springer, Singapore, 2019), Vol. 285.
[22]Z. Batool *et al.*, "Bismuth-containing III–V semiconductors: Epitaxial growth and physical properties," in *Molecular Beam Epitaxy*, edited by M. Henini (Elsevier, Oxford, 2013), Chap. 7, pp. 139–158.
[23]M. D. Johnson, C. Orme, A. W. Hunt, D. Graff, J. Sudijono, L. M. Sander, and B. G. Orr, Phys. Rev. Lett. **72**, 116 (1994).
[24]M. G. Lagally and Z. Zhang, Nature **417**, 907 (2002).
[25]J. Y. Tsao, "Surface morphology," in *Materials Fundamentals of Molecular Beam Epitaxy*, edited by J. Y. Tsao (Academic Press, San Diego, 1993), Chap. 6, pp. 201–257.
[26]J. A. Venables and G. D. T. Spiller, "Nucleation and growth of thin films," in *Surface Mobilities on Solid Materials: Fundamental Concepts and Applications, NATO Advanced Science Institutes Series*, edited by V. T. Binh (Springer US, Boston, MA, 1983), pp. 341–404.
[27]M. Załuska-Kotur, H. Popova, and V. Tonchev, Crystals **11**, 1135 (2021).
[28]R. L. Schwoebel and E. J. Shipsey, J. Appl. Phys. **37**, 3682 (1966).
[29]J. Villain, J. Phys. I France **1**, 19 (1991).
[30]G. S. Bales and A. Zangwill, Phys. Rev. B **41**, 5500 (1990).
[31]R. Rangdee and P. Chatraphorn, Surf. Sci. **600**, 914 (2006).
[32]J. G. Amar and F. Family, MRS Online Proceedings Library **440**, 229 (1996).
[33]J. P. DeVita, L. M. Sander, and P. Smereka, "Quasicontinuum Monte Carlo simulation of multilayer surface growth," in *Multiscale Modeling in Epitaxial Growth, ISNM International Series of Numerical Mathematics*, edited by A. Voigt (Birkhäuser, Basel, 2005), pp. 57–66.
[34]F. F. Leal, S. C. Ferreira, and S. O. Ferreira, J. Phys.: Condens. Matter **23**, 292201 (2011).

[35]M. Vladimirova, A. Pimpinelli, and A. Videcoq, J. Cryst. Growth **220**, 631 (2000).
[36]M. Rost, P. Šmilauer, and J. Krug, Surf. Sci. **369**, 393 (1996).
[37]C. Duport, P. Politi, and J. Villain, "Growth instabilities in MBE," in *Quantum Mechanics to Technology* (Springer, Berlin, Heidelberg, 1996), pp. 213–230.
[38]C. Misbah, O. Pierre-Louis, and Y. Saito, Rev. Mod. Phys. **82**, 981 (2010).
[39]M. A. Stevens, K. A. Grossklaus, and T. E. Vandervelde, J. Cryst. Growth **527**, 125216 (2019).
[40]O. Pierre-Louis and C. Misbah, Phys. Rev. Lett. **76**, 4761 (1996).
[41]C. Ratsch, M. C. Wheeler, and M. F. Gyure, Phys. Rev. B **62**, 12636 (2000).
[42]S. J. Liu, H. Huang, and C. H. Woo, Appl. Phys. Lett. **80**, 3295 (2002).
[43]L. M. Murray, A. Yildirim, S. R. Provence, D. T. Norton, T. F. Boggess, and J. P. Prineas, J. Vac. Sci. Technol. B **31**, 03C108 (2013).
[44]J. Krug and P. Kuhn, "Second layer nucleation and the shape of wedding cakes," in *Atomistic Aspects of Epitaxial Growth, NATO Science Series*, edited by M. Kotrla, N. I. Papanicolaou, D. D. Vvedensky, and L. T. Wille (Springer Netherlands, Dordrecht, 2002), pp. 145–163.
[45]S. Okumura, S. Tomabechi, R. Suzuki, Y. Matsukura, K. Tsunoda, J.-I. Kon, and H. Nishino, J. Cryst. Growth **477**, 243 (2017).
[46]N. A. K. Kaufmann, L. Lahourcade, B. Hourahine, D. Martin, and N. Grandjean, J. Cryst. Growth **433**, 36 (2016).
[47]H. Turski *et al.*, Appl. Surf. Sci. **484**, 771 (2019).
[48]J. Zhong, T. Zhang, Z. Zhang, and M. Lagally, Phys. Rev. B **63**, 113403 (2001).
[49]Y. Liu, J. V. Knutsson, N. Wilson, E. Young, S. Lehmann, K. A. Dick, C. J. Palmstrøm, A. Mikkelsen, and R. Timm, Nat. Commun. **12**, 5990 (2021).
[50]T. Tiedje and A. Ballestad, Thin Solid Films **516**, 3705 (2008).
[51]D. Kandel and E. Kaxiras, Solid State Phys. **54**, 219 (2000).